A Robust Open-Circuit Fault Diagnosis Method for Three-Phase Interleaved Boost Converter

Chuanfeng Li, *Student Member, IEEE*, Yang Yu, *Senior Member, IEEE*, Tingyan Tang, Qingxin Liu, and Xiyuan Peng

***Abstract*—An open-circuit fault will increase input current ripple and reduce the energy transmission efficiency, which will deteriorate the inherent advantages of an interleaved boost converter. To guarantee the efficient and reliable operation of a system, it is necessary to diagnose the open-circuit fault by sensing the input current. In practical application, the sampling value of the input current will be polluted by noise and disturbance, which will weaken the robustness of fault diagnosis. To address the problem, this article proposes a robust open-circuit fault diagnosis method. By theoretically deriving the input current, it can be found that the input current contains helpful information, which can be used to identify the fault phase. The proposed method extracts this useful information by sampling the input current and holding it at specific moments. Moreover, this method integrates the sampling values to enhance robustness against noise. The fault phase can quickly be detected and located by observing and comparing the integrals during two switching periods. The method has robustness against the noise and the disturbance. Additionally, the method needs no extra sensors to sense the input current, which the control loop uses. Simulations and hardware experiments are carried to prove the practicability and the robustness of the proposed method.**

***Index Terms*—Fault diagnosis, interleaved boost converter (IBC), open-circuit fault (OCF), reliability.**

I. Introduction

THE dc–dc converters are widely used in various fields, such as aerospace, communication, electric vehicles, and renewable energy power system [1]–[8]. To ensure the continuous operation for some specific applications, such as the photovoltaic system and fuel cell system, the reliability guarantee of dc–dc is vital. When a fault occurs, fault tolerance is an effective way to ensure the continuous operation of a dc–dc converter. The interleaved dc–dc converter has the ability of fault tolerance due to the inherent redundancy. In addition, with the benefits of high efficiency, high power density, low input current ripple, and low output voltage ripple [2]–[4], the interleaved topology is widely used in the PFC converter, the photovoltaic system, and the fuel cell application.

Manuscript received January 29, 2022; revised April 6, 2022; accepted April 15, 2022. Date of publication April 21, 2022; date of current version May 23, 2022. This work was supported by the National Natural Science Foundation of China under Grant 62071150. Recommended for publication by Associate Editor A. J. Marques Cardoso (GE). *(Corresponding author: Yang Yu.)*

The authors are with the School of Electronics and Information Engineering, Harbin Institute of Technology, Harbin 150080, China (e-mail: licf@hit.edu.cn; yuyanghit@hit.edu.cn; 21s005088@stu.hit.edu.cn; 20s005062@stu.hit.edu.cn; pxy@hit.edu.cn).

Color versions of one or more figures in this article are available at https://doi.org/10.1109/TPEL.2022.3169167.

Digital Object Identifier 10.1109/TPEL.2022.3169167

However, when an open-circuit fault (OCF) of the semiconductor switch occurs in a phase, the input current ripple will increase, which will damage the fuel cell. Moreover, the OCF will cause the current stress to other healthy phases so that the entire interleaved boost converter (IBC) will fail catastrophically. Therefore, it is necessary to detect the fault and locate the faulty phase as soon as possible.

As reported in [3], [8]–[11], the power semiconductor switch is one of the most fragile components in a dc–dc converter. The fault of the power semiconductor switch can be categorized as the short-circuit fault (SCF) and the OCF. Commonly, the SCFs have a great impact on the reliable and safe operation of the whole converter, and the SCF can turn into an OCF due to the protector, including fuses, circuit breakers, and internal semiconductor module protection [4]–[6]. Thus, the OCF of the semiconductor switch in a three-phase IBC is mainly considered in this article.

Much research has been devoted to detecting and identifying the OCF of the semiconductor switch in recent years [2]–[7], [9], [10], [12]–[28]. For a dc–dc converter, the fault diagnosis method can be categorized into model-based and signal-based methods.

The model-based method can diagnose the OCF by comparing the threshold and the residual, which is generated by comparing the theoretical current and the real current from the actual converter. As presented in [3], [7], [12]–[15], the OCF can be identified by comparing the inductor current estimated by the observer with the current measured by the actual inductor current sensor for per phase. To avoid using additional sensors, a state observer was established using the information already available in the closed-loop control. The OCF can be identified by analyzing and comparing the residual of the state observer on the time domain [4]. Although the model-based method can detect and identify the OCF for the IBC, complex computational effort and an accurate model are necessary to attain robustness against disturbances. The model-based methods mentioned above are not cost-saving.

Many scholars have chosen signal-based methods instead of model-based methods to diagnose OCF. The signal-based method can diagnose the OCF by extracting the feature of the commonly available variables. The features on the time-domain include the diode voltage and the inductor current derivative captured by the Rogowski coil sensor [6], the primary voltage of the transformer [9], the voltage on magnetic component [10], the voltage of the flying capacitor [16], the inductor voltage [17],

the Park's vectors of inductor current [5], [18], and the slope of the inductor current over time [19]–[26]. The frequency-domain features include the magnitude and phase angle of input current at the switching frequency [2], the frequency information in the magnetic field near the converters [27], and the harmonic amplitude and phase of the output voltage at the switching frequency [28]. The signal-based methods mentioned above can be classified as those suitable for single-phase dc–dc converter and those suitable for two-phase or multiphase interleaved dc–dc converter. Compared with the single-phase converter, the two-phase or multiphase interleaved dc–dc converter has a more complex structure. Therefore, the OCF occurring in a two-phase or multiphase converter needs to be detected as quickly as possible while it also needs to be located to a faulty phase.

For a three-phase IBC and a floating IBC, the OCF can be detected and identified using the Park's vectors in [5] and [18]. However, the technique needs to measure the inductor current per phase, increasing maintenance costs.

As reported in [24]–[26], the OCF can be diagnosed by analyzing the relationship between the input current derivative and gate signal. The method only needs to measure the input current, which is commonly used for closed-loop control. However, the input current derivative would be affected by the measurement noise. In [2], a method based on the fast Fourier transform was proposed to identify the OCF. The method can diagnose the OCF by calculating the magnitude and phase angle of switching frequency based harmonic component of total input current. Similarly, the OCF can be diagnosed based on the harmonic amplitude and phase angle of the output voltage [28]. Nevertheless, the phase angle and magnitude calculation will be affected by the phase imbalances caused by internal disturbances. In addition, the calculation of phase angle will also be affected by the noise because the noise will pollute the sampling values of the input current. The noise factors include parasitic effects, the ambient temperature effect, and the electromagnetic interference noise from the converter itself [6], [29], [30]. The noise factors and internal and external disturbances would affect the robustness of the signal-based fault diagnosis method.

To address the limitations and shortages mentioned above, a robust fault diagnosis method is proposed in this article. The proposed signal-based method samples the input current at three specific moments. It can be theoretically proved that the three sampling values are equal under healthy conditions, but there will be a difference between the three sampling values when an OCF occurs in one phase. The maximum difference can be used as the boundary of whether the fault occurs or not. Moreover, the sampling value of input current at the specific moment corresponding to the faulty phase is located in the middle of the other two sampling values corresponding to the healthy phase. The OCF can be identified by observing the sampling value of the input current. In order to reduce the influence of noise on the sampling values of the input current used for fault detection, the proposed method integrates the sampling value of the input current in two sliding time windows to reduce the influence of the noise. The proposed method is still effective when the three-phase inductor currents are imbalanced. The proposed method can diagnose the OCF in a three-phase IBC against the noise and the disturbances. Furthermore, the proposed strategy only needs to measure the total input current used in the closed-loop control scheme. Therefore, the method avoids using extra sensors, saving implementation costs.

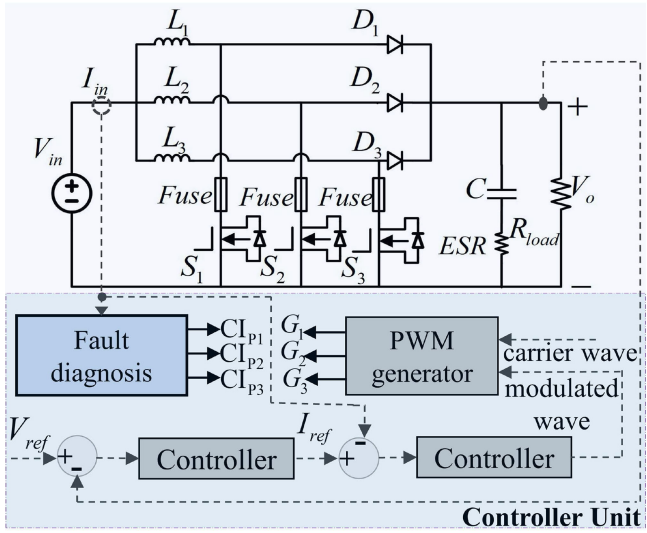

Fig. 1. Circuit diagram of the three-phase IBC with a controller unit.

The rest of this article is organized as follows. Section II introduces the operation of the three-phase IBC under the healthy condition and the faulty condition. An OCF diagnosis strategy is proposed in Section III. Section IV presents simulations and robustness analysis. The experimental results are provided to verify the effectiveness of the proposed method in Section V. Finally, Section VI concludes this article.

II. Operation of Three-Phase IBC

The topology of the three-phase IBC is shown in Fig. 1. In the three-phase IBC circuit, V_{in} represents the input voltage, L_1, L_2, and L_3 represent inductor, D_1, D_2, and D_3 are the diodes, S_1, S_2, and S_3 are the switches, C is an electrolytic capacitor, ESR represents the equivalent series resistance, R_{Load} represents a load resistor, and V_o represents the output voltage. The fuse will open the circuit just as if the conduction current exceeds the given threshold. Thus, the fuse can transfer an SCF into an OCF.

In the controller unit of the three-phase IBC circuit, the V_{ref} is the reference voltage, and the I_{ref} is the reference current. The gate signal (G_1, G_2, G_3) can be used to control switches to turn ON or OFF. The carrier wave is a sawtooth wave with a phase shift of $2\pi/3$.

In order to make the output voltage reach the reference voltage, a double closed-loop control strategy is used for a three-phase IBC. The controller uses the error between the reference voltage and the output voltage to generate the reference current. On this basis, the modulation wave can be generated by comparing the reference current and input current. By comparing the carrier wave and the modulating wave, the gate signal can be generated. Generally, the input current (I_{in}) is used in the control scheme.

A. Operation of Three-Phase IBC Under a Healthy Condition

In normal operation, the input current is equal to the sum of each phase inductor current, as shown in the following equation:

$$I_{\text{in}} = I_{L1} + I_{L2} + I_{L3} \tag{1}$$

where I_{L1}, I_{L2}, and I_{L3} represent three phase inductor currents. The inductor current will rise with the slope of V_{in}/L when the switch S_1 is turn ON, and the inductor current will fall with the slope of $(V_{\text{in}} - V_o)/L$ when the switch S_1 is turned OFF.

The first phase inductor current I_{L1} can be expressed as shown in the following equation:

$$I_{L1} = \begin{cases} \bar{I}_L - \frac{V_{\text{in}}DT}{2L} + \frac{V_{\text{in}}}{L}t & 0 < t \le DT \\ \bar{I}_L - \frac{V_{\text{in}}DT}{2L} + \frac{V_oDT}{L} + \frac{(V_{\text{in}}-V_o)}{L}t & DT < t \le T \end{cases} \tag{2}$$

where D represents the duty cycle, T represents the period, and $\bar{I}_L$ represents the average inductor current. When the three-phase IBC operates at the continuous conduction mode, the relationship between the output voltage and the input voltage can be expressed as shown in the following equation:

$$\frac{V_o}{V_{\text{in}}} = \frac{1}{1-D}. \tag{3}$$

Hence, the I_{L1} can be simplified as shown in the following equation:

$$I_{L1} = \begin{cases} \bar{I}_L - \frac{V_{\text{in}}DT}{2L} + \frac{V_{\text{in}}}{L}t & 0 < t \le DT \\ \bar{I}_L - \frac{V_{\text{in}}D(D+1)T}{2(D-1)L} - \frac{DV_{\text{in}}}{(1-D)L}t & DT < t \le T \end{cases}. \tag{4}$$

According to (4), the duty cycle determines the end of the inductor current rising and falling. It means that the duty cycle determines whether the switch is ON or OFF. According to the number of semiconductor switches, which are simultaneously active, the duty cycle can be divided into three intervals as shown in the following equations:

$$\frac{1}{3} < D < \frac{2}{3} \tag{5}$$

$$D > \frac{2}{3} \tag{6}$$

$$D < \frac{1}{3}. \tag{7}$$

For interval (5), considering the phase shift, the I_{L2} and I_{L3} can be expressed as shown in the following equations:

$$I_{L2} = \begin{cases} \bar{I}_L + \frac{V_{\text{in}}D(-3D+1)T}{6(D-1)L} + \frac{DV_{\text{in}}}{(D-1)L}t & 0 < t \le \frac{1}{3}T \\ \bar{I}_L + \frac{V_{\text{in}}(-3D-2)T}{6L} + \frac{V_{\text{in}}}{L}t & \frac{1}{3}T < t \le \left(D+\frac{1}{3}\right)T \\ \bar{I}_L - \frac{V_{\text{in}}D(3D+5)T}{6(D-1)L} + \frac{DV_{\text{in}}}{(D-1)L}t & \left(D+\frac{1}{3}\right)T < t \le T \end{cases} \tag{8}$$

$$I_{L3} = \begin{cases} \bar{I}_L + \frac{V_{\text{in}}(2-3D)T}{6L} + \frac{V_{\text{in}}}{L}t & 0 < t \le \left(D-\frac{1}{3}\right)T \\ \bar{I}_L - \frac{V_{\text{in}}D(3D+1)T}{6(D-1)L} + \frac{DV_{\text{in}}}{(D-1)L}t & \left(D-\frac{1}{3}\right)T < t \le \frac{2T}{3} \\ \bar{I}_L - \frac{V_{\text{in}}(3D+4)T}{6L} + \frac{V_{\text{in}}}{L}t & \frac{2T}{3} < t \le T \end{cases}. \tag{9}$$

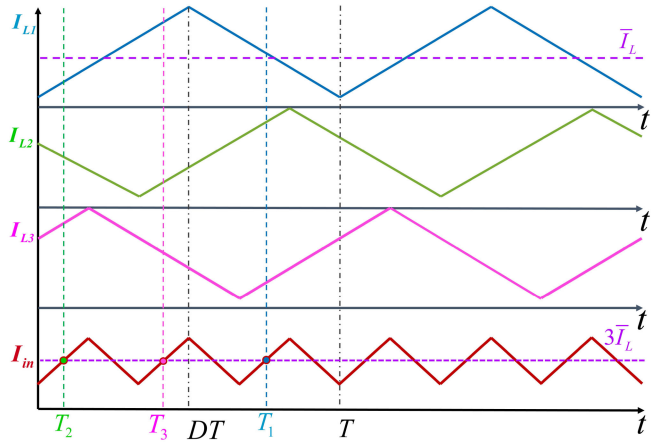

Fig. 2. Waveforms of three-phase inductor current and input current with the marking of sampling moments.

According to (1), (4), (8), and (9), the I_{in} can be rewritten as shown in the following equation:

$$I_{\text{in}} = \begin{cases} 3\bar{I}_L + \frac{V_{\text{in}}(3D-2)(-3DT+T+6t)}{6(D-1)L} & 0 < t < \left(D-\frac{1}{3}\right)T \\ 3\bar{I}_L - \frac{V_{\text{in}}(3D-1)(DT-2t)}{2(D-1)L} & \left(D-\frac{1}{3}\right)T < t < \frac{T}{3} \\ 3\bar{I}_L - \frac{V_{\text{in}}(3D-2)(3DT+T-6t)}{6(D-1)L} & \frac{T}{3} < t < DT \\ 3\bar{I}_L + \frac{V_{\text{in}}(3D-1)(DT+2T+6t)}{6(D-1)L} & DT < t < \left(D+\frac{1}{3}\right)T \\ 3\bar{I}_L - \frac{V_{\text{in}}(3D-2)(DT+T-2t)}{2(D-1)L} & \left(D+\frac{1}{3}\right)T < t < \frac{2T}{3} \\ 3\bar{I}_L - \frac{V_{\text{in}}(3D-1)(3DT+4T-6t)}{6(D-1)L} & \frac{2T}{3} < t < T \end{cases}. \tag{10}$$

In order to make the output voltage reach the reference value, it is necessary to sample and hold the average of the input current for the current loop controller. The input current will fall to the average at one-half of the off-time for the first switch, that is, T_1. The T_1 can be expressed as shown in the following equation:

$$T_1 = \frac{(DT+T)}{2} = \frac{(D+1)}{2}T. \tag{11}$$

Similarly, the input current will also reach the average at one-half of the off-time for the second and third switches, which are T_2 and T_3. Compared to T_1, T_2, and T_3, a phase shift of $2T/3$ and $T/3$ occurs, which can be expressed as shown in the following equations:

$$T_2 = \frac{(D+1)}{2}T - \frac{2T}{3} \tag{12}$$

$$T_3 = \frac{(D+1)}{2}T - \frac{T}{3}. \tag{13}$$

Fig. 2 illustrates the waveforms of the three-phase inductor current and the specific sampling moments in two switching cycles under the healthy condition. It is evident that the input current will reach the average at T_1, T_2, and T_3.

Under the healthy condition, the sampling value at three moments can be expressed as shown in the following equation:

$$I_{\text{in}}(T_1) = I_{\text{in}}(T_2) = I_{\text{in}}(T_3) = 3\bar{I}_L. \tag{14}$$

TABLE I
INPUT CURRENT AT SPECIFIC SAMPLING TIME UNDER DIFFERENT FAULTY CONDITION FOR INTERVAL (5) AND INTERVAL (6)

Fault leg	Sampling time	Input current
Phase-1 fault	$T_1=(D+1)T/2$	$2\bar{I}_L$
	$T_2=(D+1)T/2-2T/3$	$2\bar{I}_L+V_{in}T/6L$
	$T_3=(D+1)T/2-T/3$	$2\bar{I}_L-V_{in}T/6L$
Phase-2 fault	$T_1=(D+1)T/2$	$2\bar{I}_L-V_{in}T/6L$
	$T_2=(D+1)T/2-2T/3$	$2\bar{I}_L$
	$T_3=(D+1)T/2-T/3$	$2\bar{I}_L+V_{in}T/6L$
Phase-3 fault	$T_1=(D+1)T/2$	$2\bar{I}_L+V_{in}T/6L$
	$T_2=(D+1)T/2-2T/3$	$2\bar{I}_L-V_{in}T/6L$
	$T_3=(D+1)T/2-T/3$	$2\bar{I}_L$

TABLE II
INPUT CURRENT AT SPECIFIC SAMPLING TIME UNDER DIFFERENT FAULTY CONDITION FOR INTERVAL (7)

Fault leg	Sampling time	Input current
Phase-1 fault	$T_1=(D+1)T/2$	$2\bar{I}_L$
	$T_2=(D+1)T/2+T/3$	$2\bar{I}_L+DV_{in}T/3(1-D)L$
	$T_3=(D+1)T/2-T/3$	$2\bar{I}_L-DV_{in}T/3(1-D)L$
Phase-2 fault	$T_1=(D+1)T/2$	$2\bar{I}_L-DV_{in}T/3(1-D)L$
	$T_2=(D+1)T/2+T/3$	$2\bar{I}_L$
	$T_3=(D+1)T/2-T/3$	$2\bar{I}_L+DV_{in}T/3(1-D)L$
Phase-3 fault	$T_1=(D+1)T/2$	$2\bar{I}_L+DV_{in}T/3(1-D)L$
	$T_2=(D+1)T/2+T/3$	$2\bar{I}_L-DV_{in}T/3(1-D)L$
	$T_3=(D+1)T/2-T/3$	$2\bar{I}_L$

It can be found that the sampling values of input current is the same at the three specific sampling moments, and it is equal to three times the average inductor current.

B. Operation of Three-Phase IBC Under the Faulty Condition

When an OCF occurs in phase-1, the first phase inductor current will fall to zero and keep. Under the condition of the OCF in phase-1, the input current is the sum of I_{L2} and I_{L3}, expressed as shown in the following equation:

$$I_{\text{in\_}F1}=\begin{cases}2\bar{I}_L-\frac{V_{\text{in}}(3(D^2-D)T+T+3(1-2D)t)}{3(D-1)L} & 0<t<\left(D-\frac{1}{3}\right)T\\ 2\bar{I}_L+\frac{V_{\text{in}}(-D^2T+2Dt)}{(D-1)L} & \left(D-\frac{1}{3}\right)T<t<\frac{T}{3}\\ 2\bar{I}_L+\frac{V_{\text{in}}\left(-3D^2T+T+3(2D-1)t\right)}{3(D-1)L} & \frac{T}{3}<t<\frac{2T}{3}\\ 2\bar{I}_L+\frac{V_{\text{in}}(-(D+1)T+2t)}{L} & \frac{2T}{3}<t<\left(D+\frac{1}{3}\right)T\\ 2\bar{I}_L+\frac{V_{\text{in}}((2-3D(D+1))T+3(2D-1)t)}{3(D-1)L} & \left(D+\frac{1}{3}\right)T<t<T\end{cases}. \tag{15}$$

The sampling value for the input current at the three specific moments can be expressed as shown in the following equations:

$$I_{\text{in\_}F1}(T_1)=2\bar{I}_L \tag{16}$$

$$I_{\text{in\_}F1}(T_2)=2\bar{I}_L+\frac{V_{\text{in}}}{6L}T \tag{17}$$

$$I_{\text{in\_}F1}(T_3)=2\bar{I}_L-\frac{V_{\text{in}}}{6L}T. \tag{18}$$

It can be found that the sampling value of the input current at T_1 is equal to two times the average of the inductor current, in the middle of the sampling values at T_2 and T_3. The sampling time T_1 is the moment when the inductor current of the faulty phase-1 falls to its average value. It can be seen that the sampling value of the input current at specific moments can indicate the fault phase.

In the same way, the analytical expression of the input current can be derived when an OCF occurs in phase-2 or phase-3, and the sampling values of the input current are shown in Table I.

TABLE III
SPECIFICATIONS OF A THREE-PHASE IBC

Parameter	Variable	Value
Source voltage	V_{in}	12 V
Inductance	L	1 mH
Capacitance	C	370 μF
Equivalent series resistance	ESR	0.15 Ω
Duty cycle	D	0.5
Switching frequency	f_{sw}	10 kHz
Load resistance	R_{load}	4 Ω

When an OCF occurs in phase-2 or phase-3, it can be seen that the sampling value of input current at T_2 or T_3 are also located in the middle of the sampling values at the other two sampling times. It suggests that the input current contains useful information that can be used to locate the faulty phase. Therefore, this result of theoretical derivation gives us the confidence to detect and identify OCF only using the input current for the IBC.

Similarly, for interval (6) and interval (7), the analytical expression of input current also can be derived, and the sampling value can be calculated when an OCF occurs in a different phase. For interval (6), the setting of the sampling moments and the sampling values of input current are the same as that for interval (5), as shown in Table I. For interval (7), the sampling values of input current at specific sampling moments under different faulty phases are shown in Table II.

As shown in Tables II and III, it can be found that the sampling value at a specific moment corresponding to the faulty phase is located in the middle of the sampling values at the other two sampling moments corresponding to the healthy phase. It indicates that the OCF can be diagnosed by comparing the sampling values of the input current.

III. Proposed Fault Diagnosis Method

The sampling values of the input current under healthy and faulty conditions are analyzed in Section II. Under the healthy condition, the three sampling values of inductor current are the same in a switching period. And there will be a difference between the three sampling values when an OCF occurs in a phase. The maximum difference can be used as a boundary of whether the fault occurs or not. Because the input current will be polluted by noise, the maximum difference can be affected by the noise. According to [29], the random noise is Gaussian distribution for the dc–dc converter. In order to improve the noise resistance in practical application, the sampling value and holding value of the input current need to be integrated. The integral of the input current in two switching periods can be expressed as shown in the following equation:

$$\begin{aligned}\hat{I}^*_{\text{in}}(T_1) &= \sum_{i=0}^{1}(I^*_{\text{in}}(T_1)T)\\ &= (I_{\text{in}}(T_1)+N_1(0,\sigma_n^2))T+(I_{\text{in}}(T_1)+N_2(0,\sigma_n^2))T\\ &= T(2I_{\text{in}}(T_1)+\sqrt{2}\sigma_n). \end{aligned} \tag{19}$$

Here, the $I^*_{\text{in}}(T_1)$ represents the sampling value of the input current containing noise at T_1, the $\hat{I}^*_{\text{in}}(T_1)$ represents the integral of the sampling value containing noise, the $N_1(0,\sigma_n^2)$ and $N_2(0,\sigma_n^2)$ represent the noise with an average of 0 and a variance of σ_n^2. The expectation of noise is $\sqrt{2}\sigma_n$, and the expectation of the input current signal is $2I_{\text{in}}$. It can be calculated that the signal-to-noise ratio (SNR) will increase the $\sqrt{2}$ times by integrating the sampling value in two switching periods.

The sliding window integrator needs to be used to process the sampling values of the input current with noise. The length of the window is set to two switching periods, and the length of moving is set to a period. When there is an OCF in phase-1, according to (16), (17), and (18), the integration of sampling values can be expressed as shown in the following equations:

$$\hat{I}^*_{\text{in}}(T_1) = \sum_{i=0}^{1}(I^*_{\text{in}}(T_1+iT)T) \approx 4\bar{I}_L T \tag{20}$$

$$\hat{I}^*_{\text{in}}(T_2) = \sum_{i=0}^{1}(I^*_{\text{in}}(T_2+iT)T) \approx 4\bar{I}_L T - \frac{V_{\text{in}}}{3L}T^2 \tag{21}$$

$$\hat{I}^*_{\text{in}}(T_3) = \sum_{i=0}^{1}(I^*_{\text{in}}(T_3+iT)T) \approx 4\bar{I}_L T + \frac{V_{\text{in}}}{3L}T^2 \tag{22}$$

where $\hat{I}^*_{\text{in}}(T_2)$ and $\hat{I}^*_{\text{in}}(T_3)$ represent the integrals of sampling values at T_2 and T_3. The minimum difference between the three integrals of the input current can be defined as a threshold, which can be expressed as shown in the following equation:

$$\begin{aligned}I_{Th} = \min\{&\left|\hat{I}^*_{\text{in}}(T_1)-\hat{I}^*_{\text{in}}(T_2)\right|,\left|\hat{I}^*_{\text{in}}(T_1)-\hat{I}^*_{\text{in}}(T_3)\right|\\ &\left|\hat{I}^*_{\text{in}}(T_2)-\hat{I}^*_{\text{in}}(T_3)\right|\} = V_{\text{in}}T^2 3\,L.\end{aligned} \tag{23}$$

The calculated threshold in (23) applies to interval (5) and interval (6). For interval (7), the threshold can be expressed as shown in the following equation:

$$\begin{aligned}I'_{\text{Th}} = \min\{&\left|\hat{I}^*_{\text{in}}(T_1)-\hat{I}^*_{\text{in}}(T_2)\right|,\left|\hat{I}^*_{\text{in}}(T_1)-\hat{I}^*_{\text{in}}(T_3)\right|\\ &\left|\hat{I}^*_{\text{in}}(T_2)-\hat{I}^*_{\text{in}}(T_3)\right|\} = DV_{\text{in}}T^2(3(1-D)L).\end{aligned} \tag{24}$$

Once the maximum difference between the three integrals of the input current exceed the threshold, an OCF will be considered to have occurred. The OCF can be detected by comparing the maximum difference between the three integrals of the input current and the threshold. Moreover, when an OCF occurs in phase-1 of three-phase IBC, the relationship between three integral values can be expressed as shown in the following equation:

$$\hat{I}^*_{\text{in}}(T_2) < \hat{I}^*_{\text{in}}(T_1) < \hat{I}^*_{\text{in}}(T_3). \tag{25}$$

The phase corresponding to the middle of the three integrals of the input current can be regarded as a faulty phase. The faulty phase can be located by determining which of the three integrals lies in the middle.

In order to clearly show the condition of the three phases of IBC, the condition indicator (CI) for phase-1, phase-2, and phase-3 is set to 1, 2, and 3, respectively. When an OCF occurs in one of the three phases, the corresponding CI will be added 0.5. Fig. 3 shows the flowchart of the proposed fault detection and identification. The OCF in three-phase IBC can be detected and identified only using the input current, duty cycle, and period.

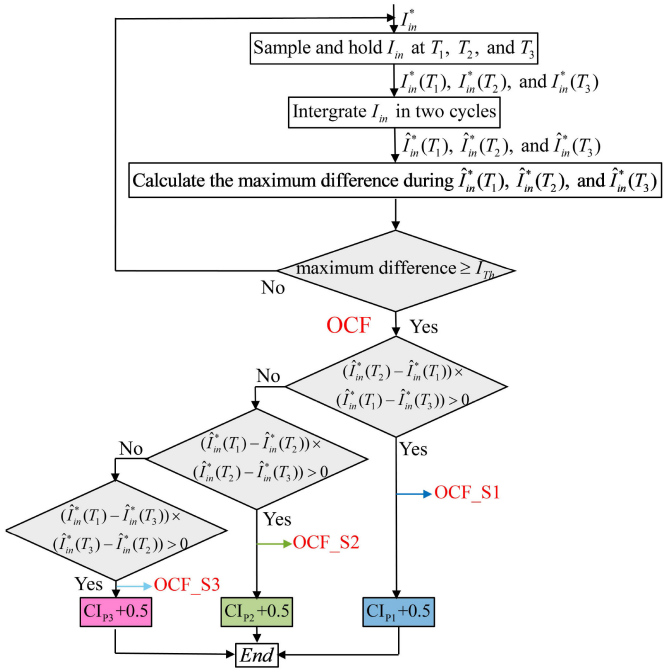

Fig. 3. Flowchart of the OCF detection and identification method.

IV. Simulation and Robustness Analysis

In order to verify the effectiveness of the proposed method, a proper simulation of three-phase IBC is established. We consider the circuit of the three-phase IBC as shown in Fig. 1. The specifications of the main parameters used in the simulation are shown in Table III.

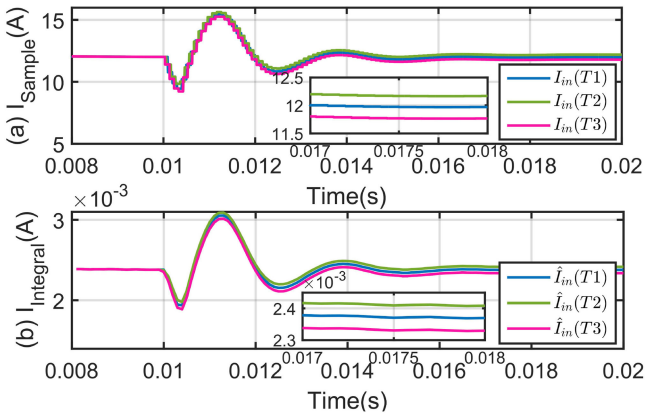

Fig. 4. Waveforms of sampling value and integral for the input current under OCF of phase-1 at $t = 0.01$ s.

A. Sampling Value and the Integral Value of Input Current

We inject an OCF in phase-1 at $t = 0.01$ s. As evident from Fig. 4, once a fault occurs, there is a significant difference between the sampling values of the input current at T_1, T_2, and T_3. The sampling value of the input current is processed using a sliding window integrator. The integral window is set to two switching periods, and the moving length is set to a switching period. There is also a significant difference between the three integrals as an OCF occurs in phase-1. In addition, the integral corresponding to the faulty phase is located in the middle of the integrals corresponding to the other two healthy phases. These results suggest that the integrals of input current can be used to detect and identify the OCF.

B. Fault Detection and Identification

Theoretically, the threshold is only related to the input voltage, inductance, and the switching frequency and is independent of other parameters of the converter. According to (23), the threshold is set to 4×10^{-5} for the validation of effectiveness and robustness of the proposed method in simulation.

Fig. 5 illustrates simulation waveforms as an OCF is injected in phase-1 of the three-phase IBC. The input current is shown in Fig. 5(a). It can be seen that the input current starts to drop when the OCF is injected at $t = 0.01$ s and quickly recovers to a stable value due to the PI closed-loop controller. Fig. 5(c) shows the threshold and maximum difference waveforms. Obviously, the maximum difference is around 0 and less than the preset threshold in a health mode and the maximum difference that exceeds the preset threshold when the OCF is injected at $t = 0.01$ s. It can be seen from Fig. 5(d) that the CI of phase-1 changes from 1 to 1.5 at $t = 0.01$ s. It suggests that the OCF can be detected, and the fault event can be located in phase-1, which is consistent with the evolution of integrals shown in Fig. 5(b).

C. Robustness Analysis Under Noise and Disturbances

When the three-phase IBC is used in practice, the noise will affect the sampling values of the input current. To prove the robustness against the noise, we add the white Gaussian noise

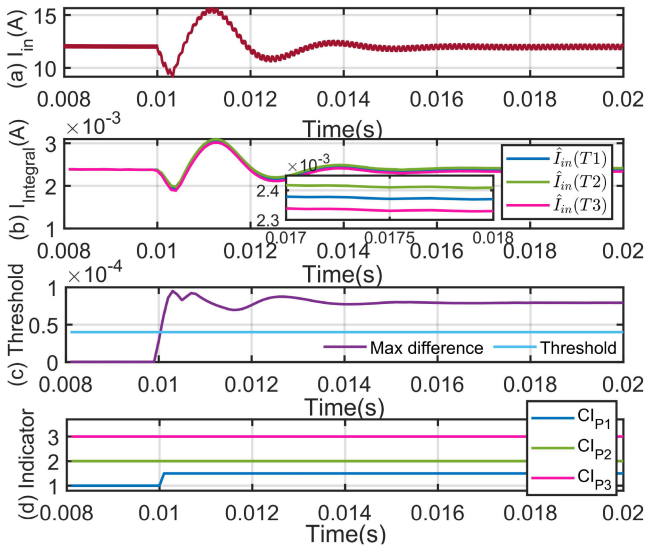

Fig. 5. Simulation waveforms under OCF of phase-1 at $t = 0.01$ s. (a) Input current. (b) Integral of input current. (c) Threshold and the maximum difference. (d) Condition indicators.

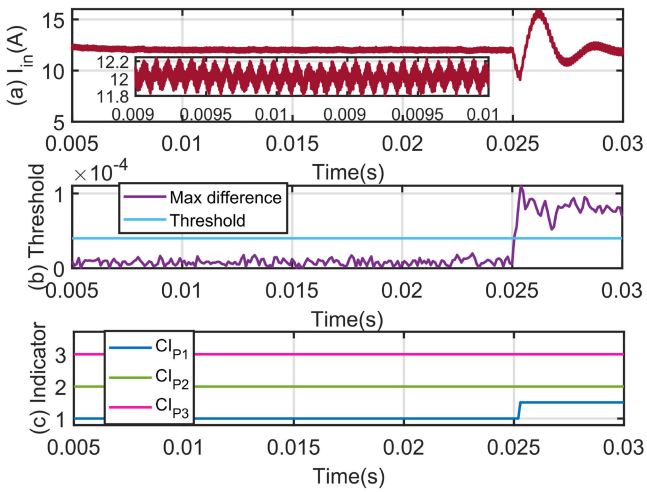

Fig. 6. Simulation waveforms when noise is added to the input current. (a) Input current. (b) Threshold and the maximum difference. (c) Condition indicators.

to the inductor current, with SNR set at 50 dB. Similarly, the threshold is set to 4×10^{-5} according to (23).

Fig. 6(a) depicts that the waveform of input current added the white Gaussian noise. It can be seen that the noise pollutes the input current. It is evident from Fig. 6(b) that the maximum difference remains below the threshold in the health mode, and the maximum difference exceeds the threshold when an OCF occurs at $t = 0.025$ s. It is suggested that no false alarms are generated. Moreover, Fig. 6(c) shows that the CI of phase-1 changes 1 to 1.5 when an OCF occurs in phase-1. It can be concluded that the OCF can still be diagnosed when the current signal is submerged by noise.

In addition, when the three-phase IBC is used in practice, the circuit parameters will deviate from the theoretical value due to the electronic and thermal stress. It will cause an imbalance

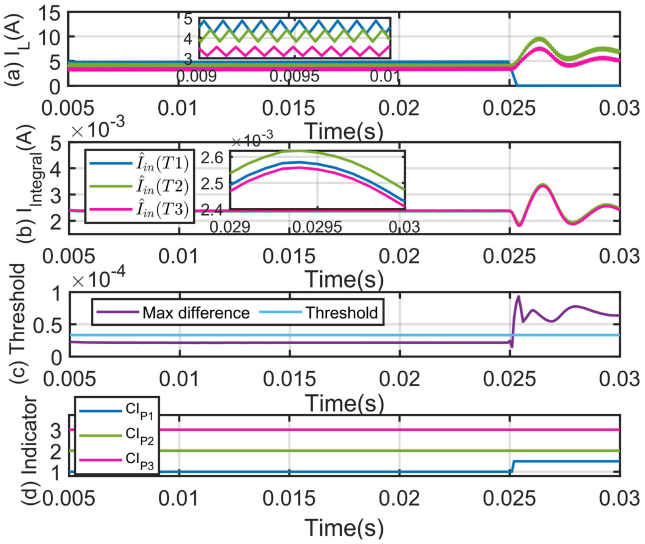

Fig. 7. Waveforms of each inductor current, the threshold and maximum difference, and the condition indicators under variations of inductance and capacitance.

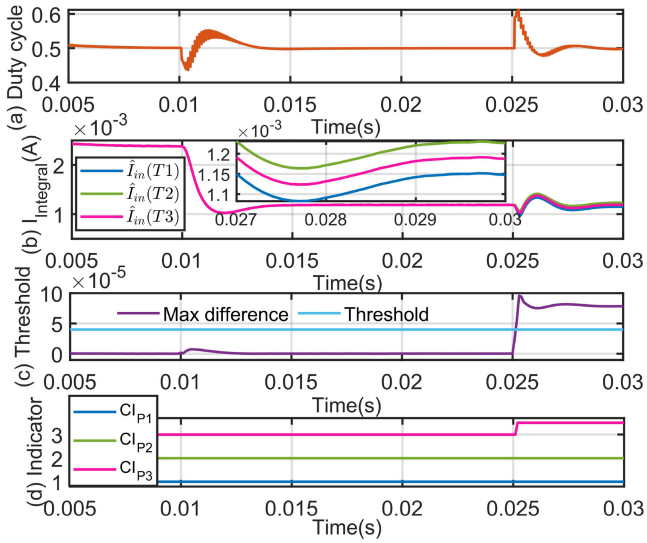

Fig. 8. Waveforms of duty cycle, integral of input current, and the condition indicators when load resistance suddenly varies.

between inductor current, especially when the three inductances vary. To verify the effectiveness of the proposed method under a variation of parameters, the tolerance of the capacitor and the inductor are set to 10%.

Fig. 7(a) shows the waveforms of each inductor current under varying inductance. It is evident that there will be an imbalance in the phase current. The threshold and maximum difference waveforms are shown in Fig. 7(c). It can be seen that the maximum difference is still less than the threshold until the OCF occurs at $t = 0.025$ s. In addition, the input current integral shown in Fig. 7(b) also implies that an OCF of phase-1 can be identified. From the fault indicator in Fig. 7(d), it can be seen that the OCF can still be located in phase-1 under imbalanced phase current.

The duty cycle and input current will be affected significantly by the load resistance and the input voltage. We vary the load resistance and input voltage to prove that the proposed method has robustness against the external distributions. The sudden step variation is set to load resistance (from 4 to 8 Ω) at $t = 0.01$ s, and the input voltage is set to increase suddenly by 40% (from 10 to 14 V) at $t = 0.01$ s. According to (23), the threshold is set to 3.3×10^{-5} when the initial voltage is set to 10 V.

In order to keep the output voltage at the reference value when the load resistance suddenly varies, the duty cycle will change significantly due to the PI double closed-loop controller, as shown in Fig. 8(a). Fig. 8(b) shows the waveform of integrals under sudden variation of load resistance. It is evident that the integrals of input current decrease significantly at $t = 0.01$ s due to the sudden variation of load resistance. From Fig. 8(c), it can be seen that the maximum difference remains below the threshold when the load step varies at $t = 0.01$ s, and the maximum difference exceeds the threshold when an OCF occurs at $t = 0.025$ s. Fig. 8(d) shows that the CI of phase-3 changes from 3 to 3.5 when an OCF is injected in phase-3 at $t = 0.025$ s. Moreover, it also can be seen that the integral of faulty phase-3 is located in the middle of the other two health phases. It suggests that the

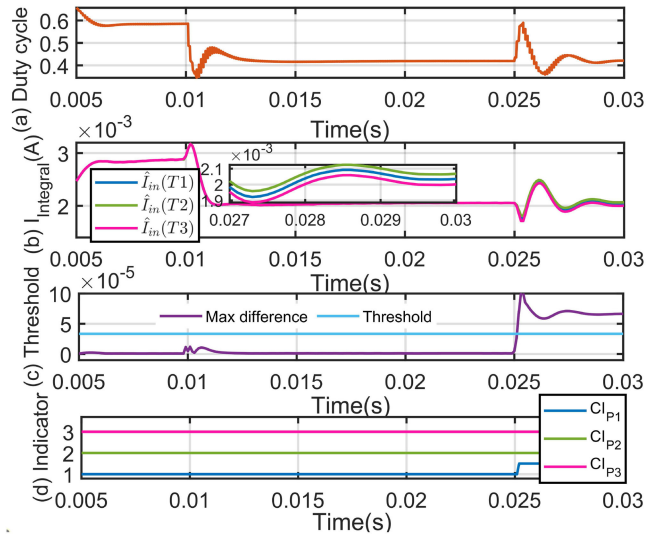

Fig. 9. Waveforms of duty cycle, integral of input current, and the condition indicators when input voltage suddenly varies.

OCF can be successfully diagnosed, although the load resistance changes suddenly and the duty cycle dynamic changes. This is because the threshold and the difference between the three integrals are not affected by a sudden load variation.

As shown in Fig. 9(a), the duty cycle will be changed from 0.6 to 0.4 when the input voltage changes from 10 to 14 V at $t = 0.01$ s. Furthermore, as shown in Fig. 9(c), the maximum difference will change when the input voltage step changes at $t = 0.01$ s but is still less than the threshold value without generating a false alarm. Fig. 9(b) and (d) show that the OCF can be successfully identified when the OCF is injected in phase-1 at $t = 0.025$ s, although the input voltage and duty cycle change significantly.

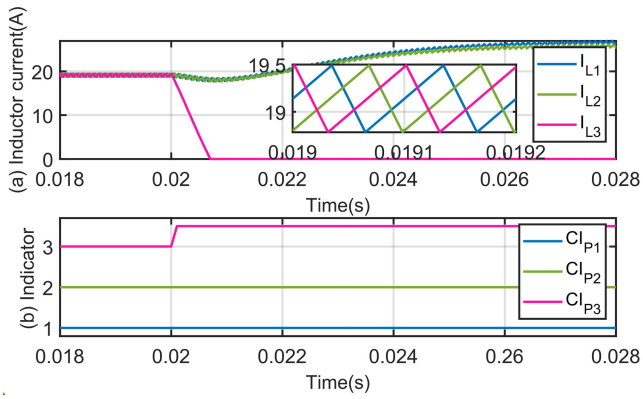

Fig. 10. Waveforms of each inductor current and the condition indicators in interval (6).

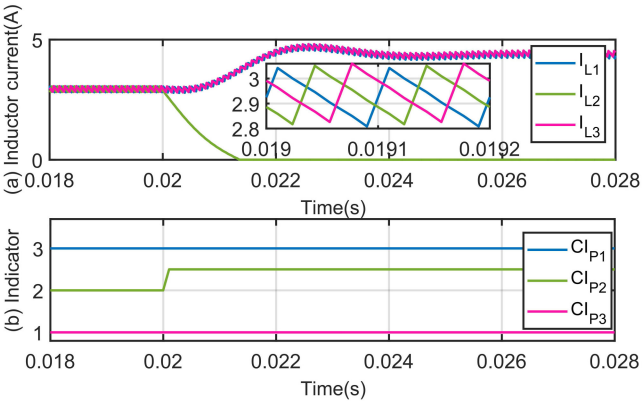

Fig. 11. Waveforms of each inductor current and the condition indicators in interval (7).

The above fault diagnosis results show that the proposed method has strong robustness against noise and external disturbances and immunity against variation of parameter.

D. Fault Diagnosis in Different Intervals

All the above simulations and analysis are for interval (5), where D is greater than one-third and less than two-thirds. Based on the analysis in Section II, it can be concluded that the duty cycle will affect the number of switches that are simultaneously active. To verify the effectiveness of the proposed method, when the duty cycle is located in various intervals, the duty cycle is set to 0.7, which is located in interval (6). According to (23), the threshold is theoretically calculated as 1×10^{-5} for interval (6).

The waveform of three-phase inductor currents is shown in Fig. 10(a) when the D is set to 0.7. It can be seen that all three switches are activated simultaneously. The OCF in phase-3 can still be detected and located when the duty cycle is greater than two-thirds.

When D is less than one-third, the sampling moments and the sampling values of input current will vary, as shown in Table II. For interval (7), the threshold is theoretically calculated as 1×10^{-5} by (24). The waveform of three-phase inductor currents and the result of fault diagnosis are shown in Fig. 11 when the D is set to 0.2. It is evident that there is no switch activated simultaneously. The CI of phase-2 changes from 2 to 2.5 as the OCF is injected at $t = 0.02$ s. It indicates that the OCF can still be diagnosed using the proposed method when the duty cycle is in different intervals.

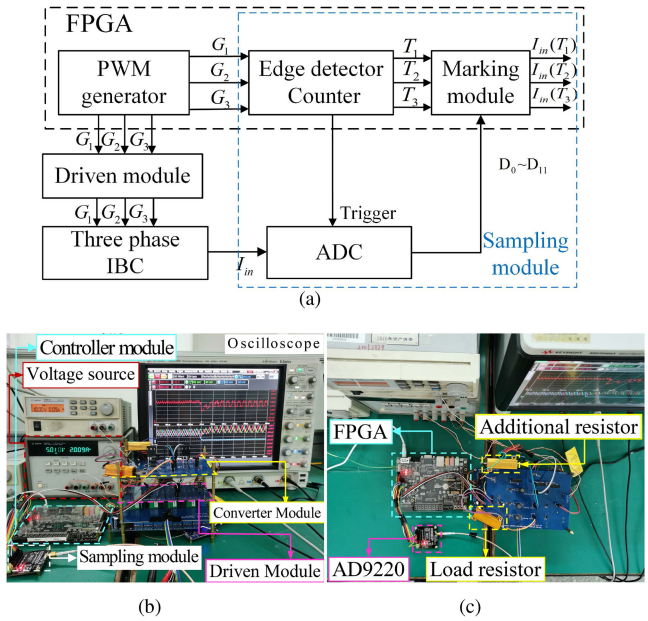

Fig. 12. Experimental prototype of three-phases IBC. (a) Block diagram. (b) Front view. (c) Top view.

TABLE IV
EXPERIMENTAL SETUP SPECIFICATIONS OF A THREE-PHASE IBC

Parameter	Value
Input voltage	5.01 V
Switching frequency	20 kHz
Inductor	100 μH
Capacitance	10 μF
Load resistance	5 Ω
Duty cycle	0.5

V. EXPERIMENTS

To verify the effectiveness of the proposed method, a laboratory prototype of a three-phase IBC was set up, as shown in Fig. 12. The prototype is composed of the controller module, the driven module, the converter module, and the sampling module. The three-phase IBC was established with the converter parameters shown in Table IV. MOSFET-IRFP250 N and the diode-1N4001 were used as power devices in IBC. The field programmable gate array was used as a controller to generate a three-phase interleaved gate signal. We used the current sensor to measure the input current and the three-phase inductor current. In practical application, only the total input current for closed-loop control needs to be measured without additional sensors. In the sampling module, we used the AD9220 to sample the input current signal from the current sensor. The AD9220 was controlled by the trigger unit, which is composed of the edge

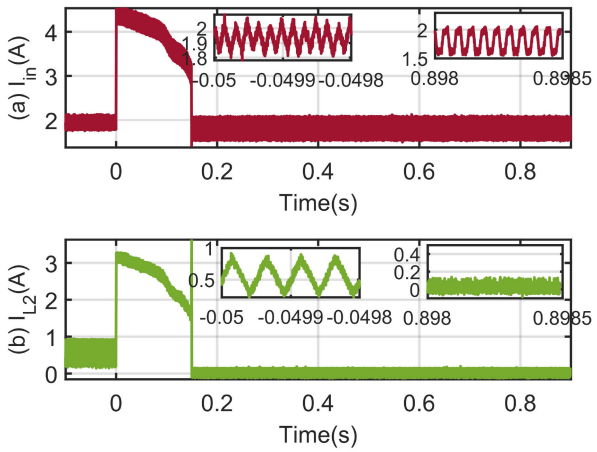

Fig. 13. Experimental waveforms when an SCF occurs at phase-2. (a) Waveform of input current. (b) Waveform of inductor current.

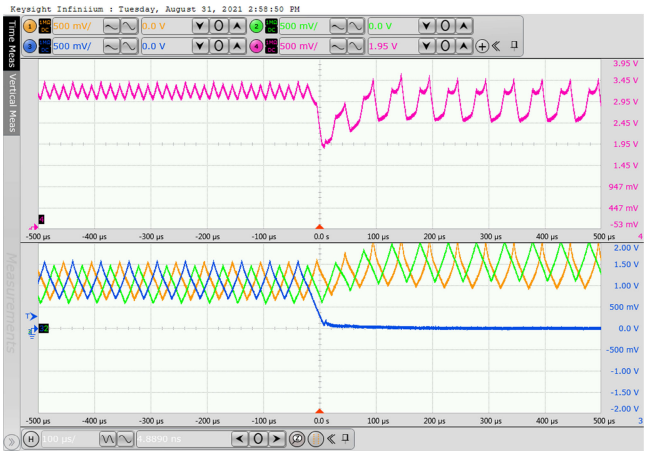

Fig. 14. Waveforms of the three-phase inductor current (500 mA/div) and input current (500 mA/div) under OCF of phase-3; time scale = 100 μs/div.

detector and the counter. The marking module was used to mark the digitized input current sent by AD9220 at specific moments. The waveform of the three-phase inductor currents and the input current were displayed in the oscilloscope.

In this article, the OCF of the switch is only considered because the SCF will turn into the OCF due to the protector, according to [4]–[6]. In order to verify this assumption, an SCF is injected in phase-2 of the IBC. The input voltage is set to 3.5 V and the fuse is selected to fast-below fuse.

Fig. 13 shows the waveforms of input current and inductor current when an SCF occurs in phase-2. It is evident that the inductor current and input current rise sharply once an SCF occurs. Due to the fuse blowing, the inductor current is reduced from 3 to 0 A within 0.15 s. It is evident from Fig. 13(a) that the SCF will turn into OCF due to the fuse.

In the hardware experiment, the length of sliding integral window is set to two switching periods in order to obtain a strong robustness. Fig. 14 shows the waveforms of the three-phase inductor currents and the input current when an OCF is injected in phase-3. It is evident that there is noise in the sampling values of the input current.

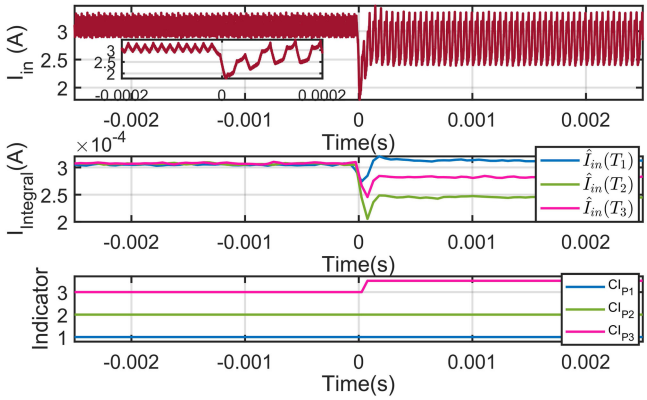

Fig. 15. Waveforms of input current, integral of input current and the condition indicators under OCF of phase-3.

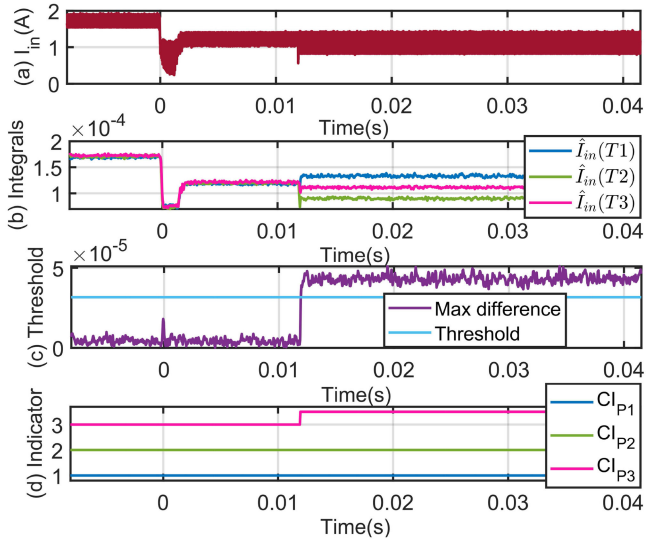

Fig. 16. Experimental waveforms when the load varies suddenly. (a) Input current. (b) Integral of input current. (c) Threshold and the maximum difference. (d) Condition indicators.

According to (23), the threshold is set to 4.2×10^{-5}. Fig. 15 shows that the integral of phase-3 is located in the middle of the other two health phases. The OCF can be located in phase-3, as depicted in Fig. 15. Although there is noise form measurement, and inherent commutation, the OCF can be successfully detected and identified.

To verify the robustness of the proposed method against external disturbances, a 5 Ω resistor was connected in series with the load using a relay switch. The load resistance changed from 5 to 10 Ω under the healthy condition. The input voltage is set to 3.8 V, and the threshold is calculated as 3.2×10^{-5}, according to (23).

Fig. 16(a) shows that the input current changes significantly due to the load step variation. The input current first decreases to close to 0 and then increases to a lower level because the load circuit is momentarily open when the relay switches the load. The CIs in Fig. 16(d) show that the proposed method can locate the fault in phase-3, which is consistent with the integral presented in Fig. 16(b). The waveforms of threshold and maximum

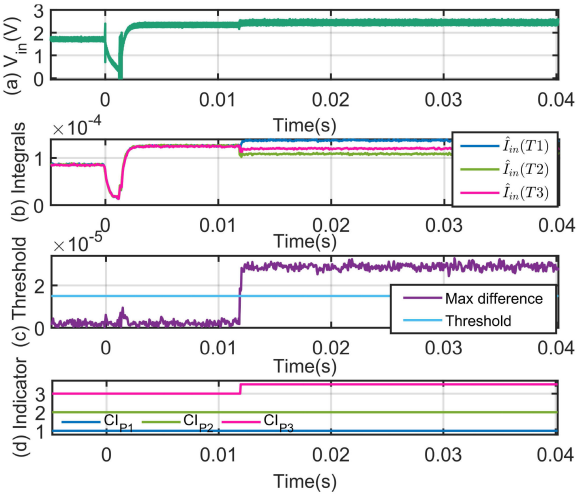

Fig. 17. Experiment waveforms when the input voltage varies suddenly. (a) Input voltage. (b) Integral of input current. (c) Threshold and the maximum difference. (d) Condition indicators.

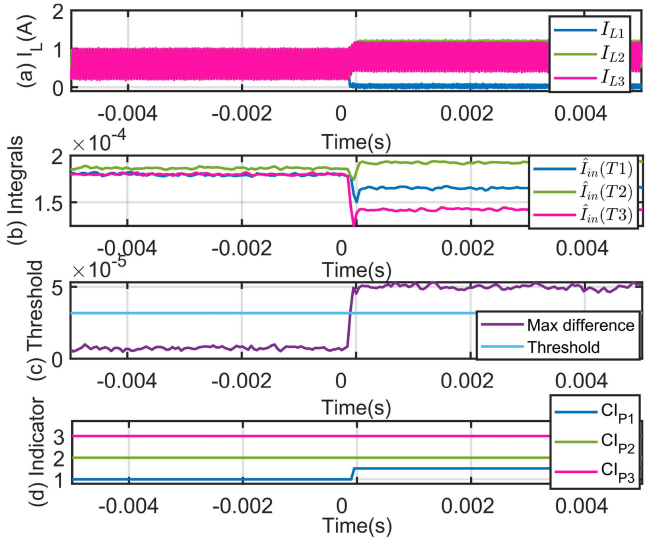

Fig. 18. Experiment waveforms under variation of inductance. (a) Inductor current. (b) Integral of input current. (c) Threshold and the maximum difference. (d) Condition indicators.

difference are shown in Fig. 16(c). It can be seen that although there is a jump in the maximum difference due to sudden load variation and relay switching, the maximum difference is still less than the preset threshold without generating a false alarm. It can be concluded that the proposed method has strong robustness against the load variation.

To verify the effectiveness of the proposed method under variation of input voltage, the input voltage is set to change by 40% (from 1.75 to 2.44 V) by the relay switching. The threshold is set to 1.46×10^{-5} according to (23).

Fig. 17 shows the experiment waveform when input voltage varies under the healthy condition. The input voltage first decreases to 0 and then increases because the power supply circuit will be in an open-circuit state for an instant when the input voltage is changed by the relay switching. As it can be observed, the maximum difference is still less than the threshold, although there is a jump in the maximum difference when the input voltage increases. It can be noted that the OCF can be successfully located in phase-3, as shown in Fig. 17(d). It is suggested that the proposed method has good robustness against voltage disturbance.

The deviation of the inductance will cause an imbalance to occur in the three-phase inductor current. In order to evaluate the robustness against inductor current imbalance due to the inductance variation, the three inductance values are selected as 100, 90, and 110 mH, respectively. The input voltage is set to 3.8 V, and the threshold is calculated as 3.2×10^{-5}, according to (23).

Fig. 18(c) depicts the maximum difference and threshold waveforms. It is evident that the maximum difference deviates from zero but is still less than the threshold without generating a false alarm. The fault diagnosis results in Fig. 18(d) show that the OCF was successfully located in phase-1, which agrees with the inductor current presented in Fig. 18(a). It can be concluded that the proposed method has strong immunity against parameter variation.

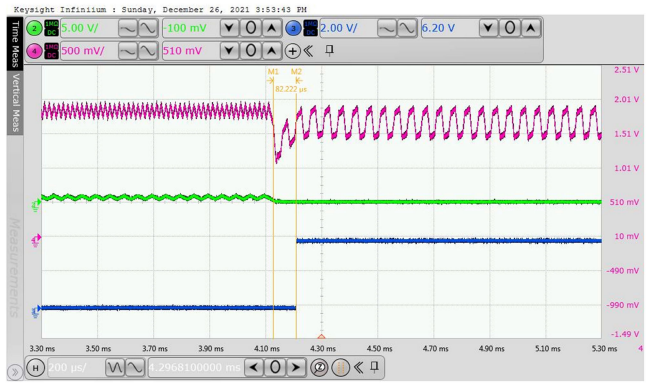

Fig. 19. Waveforms of input current (500 mA/div), inductor current of phase-1 (5 A/div), and indicator under OCF in phase-1; time scale = 200 μs/div.

In order to evaluate fault diagnosis time, an OCF is injected in phase-1, and the indicator is set to jump from low to high when an OCF is diagnosed by the proposed method. Fig. 19 depicts the waveforms of input current, inductor current of phase-1, and the indicator. It can be seen that the fault diagnosis time is 82.22 μs, which is less than two switching periods (100 μs). The proposed method has a good balance between fault diagnosis time and robustness.

Table V compares the latest fault diagnosis methods in the literature for the interleaved dc–dc converter. The proposed method requires only one current sensor to measure the input current compared with the model-based method. In addition, the sampling rate of the proposed method is the same level as that used for the closed-loop controller. It can be directly implemented in a digital controller, avoiding extra sensors and reducing implementation costs. Compared with the signal-based method, the proposed method has strong robustness against load and input voltage disturbance and has immunity to deviations of inductance and capacitance from normal values. The proposed

TABLE V
COMPARISON OF EXISTING METHODS FOR OPEN CIRCUIT FAULT DIAGNOSIS IN INTERLEAVED DC–DC CONVERTER

	Ref	Diagnosis criterion	Switching frequency	Sampling time	Max fault diagnosis time	Signals requirement	Considering the external and internal disturbance
Model-based method	[3]	Luenberger observer	25 kHz	20 μs	2 T_s[1]	Inductor current	Load, inductance, and capacitance
	[4]	Linear observer	25 kHz	0.67 μs	2 T_s[1]	Input current	Reference and load
	[7]	Sliding mode observer	25 kHz	20 μs	2 T_s[1]	Inductor current	Load, inductance, and capacitance
	[13]	Immersion and invariant observers	25 kHz	50 kHz	1.5 T_s[1]	Inductor current	Capacitance and inductance
	[15]	Immersion and invariant observers	25 kHz	20 μs	2 T_s[1]	Inductor current	Load and input voltage
Signal-based method	[2]	Switching frequency component of input current	10 kHz	33 μs	1 T_s[1]	Input current	Different irradiance level
	[16]	Inductor voltage	40 kHz	_[2]	1 T_s[1]	Inductor voltage	_[2]
	[25]	Input current derivative	{1,3,5} kHz	20 μs	2 T_s[1]	Input current	Load switching frequency
	Pro[3]	**Sampling moments at specific moments**	**20 kHz**	**16.7 μs**	**2 T_s[1]**	**Input current**	**Noise, input voltage, load, variation of capacitance, and inductance.**

[1]Switching period [2]Not specific [3]Proposed method

method has superior advantages in robustness against disturbances and reduces implementation costs.

VI. CONCLUSION

This article presents a robust fault diagnosis method applied to an IBC. An OCF of the semiconductor switch in IBC can be diagnosed by observing and comparing the integral of the input current. Thanks to the sliding window integrator, the proposed method can enhance the robustness against noise and disturbance. The simulation and the hardware experiment prove the practicability and robustness of the proposed method. Although there is a significant disturbance due to sudden load and input voltage changes and the sampling value of input current contains noise in the experiment, the OCF can be detected and identified within two switching periods, which suggests the proposed method has robustness against the noise and disturbance. In addition, the OCF can be diagnosed only by sampling the total input current at three specific moments, which is commonly used in closed-loop control. This method avoids the use of extra sensors, saving implementation costs.

REFERENCES

[1] H. Wang, X. Pei, Y. Wu, and Y. Kang, "A general fault-tolerant operation strategy under switch fault for modular series-parallel DC-DC converter," *IEEE Trans. Emerg. Sel. Topics Power Electron.*, vol. 9, no. 1, pp. 872–884, Feb. 2020.

[2] M. W. Ahmad, N. B. Y. Gorla, H. Malik, and S. K. Panda, "A fault diagnosis and postfault reconfiguration scheme for interleaved boost converter in PV-based system," *IEEE Trans. Power Electron.*, vol. 36, no. 4, pp. 3769–3780, Apr. 2021.

[3] S. Zhuo, A. Gaillard, L. Xu, C. Liu, D. Paire, and F. Gao, "An observer-based switch open-circuit fault diagnosis of DC-DC converter for fuel cell application," *IEEE Trans. Ind. Appl.*, vol. 56, no. 3, pp. 3159–3167, May/Jun. 2020.

[4] N. Wassinger, E. Penovi, R. G. Retegui, and S. Maestri, "Open-circuit fault identification method for interleaved converters based on time-domain analysis of the state observer residual," *IEEE Trans. Power Electron.*, vol. 34, no. 4, pp. 3740–3749, Apr. 2019.

[5] D. Guilbert, A. N'Diaye, A. Gaillard, and A. Djerdir, "Fuel cell systems reliability and availability enhancement by developing a fast and efficient power switch open-circuit fault detection algorithm in interleaved DC/DC boost converter topologies," *Int. J. Hydrog. Energy*, vol. 41, no. 34, pp. 15505–15517, Mar. 2016.

[6] H. Givi, E. Farjah, and T. Ghanbari, "A comprehensive monitoring system for online fault diagnosis and aging detection of non-isolated DC-DC converters' components," *IEEE Trans. Power Electron.*, vol. 34, no. 7, pp. 6858–6875, Jul. 2019.

[7] S. Zhuo, L. Xu, A. Gaillard, Y. Huangfu, D. Paire, and F. Gao, "Robust open-circuit fault diagnosis of multi-phase floating interleaved DC-DC boost converter based on sliding mode observer," *IEEE Trans. Transp. Electrific.*, vol. 5, no. 3, pp. 638–649, Sep. 2019.

[8] H. Wang, M. Liserre, and F. Blaabjerg, "Toward reliable power electronics: Challenges, design tools, and opportunities," *IEEE Ind. Electron. Mag.*, vol. 7, no. 2, pp. 17–26, Jun. 2013.

[9] X. Pei, S. Nie, Y. Chen, and Y. Kang, "Open-circuit fault diagnosis and fault-tolerant strategies for full-bridge DC-DC converters," *IEEE Trans. Power Electron.*, vol. 27, no. 5, pp. 2550–2565, May 2012.

[10] S. Nie, X. Pei, Y. Chen, and Y. Kang, "Fault diagnosis of PWM DC-DC converters based on magnetic component voltages equation," *IEEE Trans. Power Electron.*, vol. 29, no. 9, pp. 4978–4988, Sep. 2014.

[11] S. Yang, A. Bryant, P. Mawby, D. Xiang, L. Ran, and P. Tavner, "An industry-based survey of reliability in power electronic converters," *IEEE Trans. Ind. Appl.*, vol. 47, no. 3, pp. 1441–1451, May/Jun. 2011.

[12] S. Zhuo, A. Gaillard, L. Xu, C. Liu, D. Paire, and F. Gao, "Observer-based robust switch open-circuit fault diagnosis of DC-DC converter for fuel cell application," in *Proc. IEEE Ind. Appl. Soc. Annu. Meeting*, 2019, pp. 1–6.

[13] L. Xu, R. Ma, S. Zhuo, R. Xie, X. Wang, and Y. Huangfu, "Observer based switch open-circuit diagnosis for interleaved boost converter," in *Proc. IECON*, 2020, pp. 5012–5017.

[14] J. Poon, P. Jain, I. C. Konstantakopoulos, C. Spanos, S. K. Panda, and S. R. Sanders, "Model-based fault detection and identification for switching power converters," *IEEE Trans. Power Electron.*, vol. 32, no. 2, pp. 1419–1430, Feb. 2017.

[15] L. Xu, R. Ma, R. Xie, J. Xu, Y. Huangfu, and F. Gao, "Open-circuit switch fault diagnosis and fault-tolerant control for output-series interleaved boost DC-DC converter," *IEEE Trans. Transp. Electrific.*, vol. 7, no. 4, pp. 2054–2066, Dec. 2021.

[16] H. Sheng, F. Wang, and C. W. Tipton IV, "A fault detection and protection scheme for three-level DC-DC converters based on monitoring flying capacitor voltage," *IEEE Trans. Power Electron.*, vol. 27, no. 2, pp. 685–697, Feb. 2012.

[17] Z. Liu, Z. Xu, and X. Zhang, "A novel real-time fast fault-tolerance diagnosis and fault adjustment strategy for m-phase interleaved boost converter," *IEEE Access*, vol. 9, pp. 11776–11786, 2021.

[18] D. Guilbert, A. N'Diaye, A. Gaillard, and A. Djerdir, "Reliability improvement of a floating interleaved DC/DC boost converter in a PV/fuel cell stand-alone power supply," *EPE J.*, vol. 29, no. 2, pp. 49–63, Aug. 2018.
[19] M. Shahbazi, E. Jamshidpour, P. Poure, S. Saadate, and M. R. Zolghadri, "Open-and short-circuit switch fault diagnosis for nonisolated DC-DC converters using field programmable gate array," *IEEE Trans. Ind Electron.*, vol. 60, no. 9, pp. 4136–4146, Sep. 2013.
[20] E. Jamshidpour, P. Poure, E. Gholipour, and S. Saadate, "Single-switch DC-DC converter with fault-tolerant capability under open-and short-circuit switch failures," *IEEE Trans. Power Electron*, vol. 30, no. 5, pp. 2703–2712, May 2015.
[21] E. Jamshidpour, M. Shahbazi, S. Saadate, P. Poure, and E. Gholipour, "FPGA based fault detection and fault tolerance operation in DC-DC converters," in *Proc. Int. Symp. Power Electron., Electr. Drives, Autom. Motion*, 2014, pp. 37–42.
[22] E. Ribeiro, A. M. Cardoso, and C. Boccaletti, "Fault diagnosis in unidirectional non-isolated DC-DC converters," in *Proc. IEEE Energy Convers. Congr. Expo.*, 2014, pp. 1140–1145.
[23] E. Jamshidpour, P. Poure, and S. Saadate, "Photovoltaic systems reliability improvement by real-time FPGA-based switch failure diagnosis and fault-tolerant DC-DC converter," *IEEE Trans. Ind Electron.*, vol. 62, no. 11, pp. 7247–7255, Nov. 2015.
[24] E. Ribeiro, A. J. M. Cardoso, and C. Boccaletti, "Open-circuit fault diagnosis in interleaved DC-DC converters," *IEEE Trans. Power Electron.*, vol. 29, no. 6, pp. 3091–3102, Jun. 2014.
[25] F. Bento and A. J. M. Cardoso, "Open-circuit fault diagnosis in interleaved DC-DC boost converters and reconfiguration strategy," in *Proc. IEEE Int. Symp. Diagn. Electr. Mach., Power Electron. Drives*, 2017, pp. 394–400.
[26] F. Bento and A. J. M. Cardoso, "Open-circuit fault diagnosis and fault tolerant operation of interleaved DC-DC boost converters for homes and offices," *IEEE Trans. Ind. Appl.*, vol. 55, no. 5, pp. 4855–4864, Sep./Oct. 2019.
[27] Y. Chen, X. Pei, S. Nie, and Y. Kang, "Monitoring and diagnosis for the DC-DC converter using the magnetic near field waveform," *IEEE Trans. Ind Electron.*, vol. 58, no. 5, pp. 1634–1647, May 2011.
[28] P. Li, X. Li, and T. Zeng, "A fast and simple fault diagnosis method for interleaved DC-DC converters based on output voltage analysis," Electronics, vol. 10, no. 12, Jun. 2021, Art. no. 1451.
[29] A. Sangswang and C. O. Nwankpa, "Noise characteristics of DC-DC boost converters: Experimental validation and performance evaluation," *IEEE Trans. Ind Electron.*, vol. 51, no. 6, pp. 1297–1304, Dec. 2004.
[30] K. Koo, J. Kim, M. Kim, and J. Kim, "Impact of PCB design on switching noise and EMI of synchronous DC-DC buck converter," in *Proc. IEEE Int. Symp. Electromagn. Compat.*, 2010, pp. 67–71.

Chuanfeng Li (Student Member, IEEE) was born in Inner Mongolia, China, in 1996. He received the B.S. degree in automation from Inner Mongolia University, Hohhot, China, in 2019. He is currently working toward the Ph.D. degree in information and communication engineering with the Harbin Institute of Technology, Harbin, China.

His research interests include condition monitoring of power semiconductor device and fault diagnosis for power electronic converter.

Yang Yu (Senior Member, IEEE) received the B.S., M.S., and Ph.D. degrees in instrumentation science and technology from the Department of Automatic Test and Control, Harbin Institute of Technology (HIT), Harbin, China, in 2002, 2004, and 2008, respectively.

She is currently a Full Professor with the Department of Test and Control Engineering, School of Electronics and Information Engineering, HIT. Her current research interests include automatic testing, test technology for 3-D ICs, and diagnostic and prognostics for electronics and electrical systems.

Tingyan Tang received the B.S. degree in measurement and control technology and instrumentation in 2021 from the Harbin Institute of Technology, Harbin, China, where she is currently working toward the M.S. degree in information and communication engineering with the Department of Information and Communication Engineering.

Her current research interests include fault diagnosis of electronic components and integrated circuit testing technology.

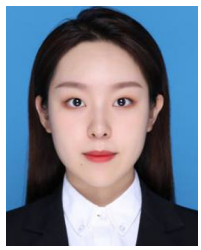

Qingxin Liu received the B.S. degree in measurement and control technology and instrumentation in 2020 from the Harbin Institute of Technology, Harbin, China, where she is currently working toward the M.S. degree in information and communication engineering with the Department of Information and Communication Engineering.

Her current research interests include automatic test technologies and fault diagnosis for electronics.

Xiyuan Peng received the Ph.D. degree in instrumentation science and technology from the Harbin Institute of Technology, Harbin, China, in 1992.

He is currently a Full Professor with the Department of Test and Control Engineering, School of Electronics and Information Engineering, Harbin Institute of Technology. His current research interests include automatic test technologies, advanced diagnostics, and prognostics.